Inorg. Chem. **2008**, *47*, 7545−7555

Experimental and Theoretical Study of the Antisymmetric Magnetic Behavior of Copper *inverse*-9-Metallacrown-3 Compounds

Tereza Afrati,[†] Catherine Dendrinou-Samara,[†] Catherine Raptopoulou,[‡] Aris Terzis,[‡] Vassilis Tangoulis,*[,†] Athanassios Tsipis,*[,||] and Dimitris P. Kessissoglou*[,†]

Department of Chemistry, Aristotle University of Thessaloniki, Thessaloniki 54124, Greece, NCSR "Demokritos", Institute of Materials Science, 15310 Aghia Paraskevi Attikis, Greece, and Laboratory of Inorganic and General Chemistry, Department of Chemistry, University of Ioannina, 45110 Ioannina, Greece

Received February 21, 2008

Use of $PhPyCNO^-/X^-$ "blends" (PhPyCNOH = phenyl 2-pyridyl ketoxime; X^- = OH^-, alkanoato, ClO_4^-) in copper chemistry yielded trinuclear clusters that have been characterized as *inverse*-9-metallacrown-3 compounds and accommodate one or two guest ligands. The magnetic behavior showed a large antiferromagnetic interaction and a discrepancy between the low-temperature magnetic behavior observed experimentally and that predicted from a magnetic model. The discrepancy between the Brillouin curve and the experimental result provides clear evidence of the influence of the antisymmetric interaction. Introducing the antisymmetric terms derived from the fit of the susceptibility data into the magnetization formula caused the simulated curve to become nearly superimposable on the experimental one. The EPR data indicated that the compound $[Cu_3(PhPyCNO)_3(\mu_3\text{-}OH)(2,4,5\text{-}T)_2]$ (**1**), where 2,4,5-T is 2,4,5-trichlorophenoxyacetate, has isosceles or lower magnetic symmetry ($\delta \neq 0$), that antisymmetric exchange is important ($\mathbf{G} \neq 0$), and that $\Delta E > h\nu$. The structures of the complexes **1** and $[Cu_3(PhPyCNO)_3(\mu_3\text{-}OH)(H_2O)(ClO_4)_2]$ (**2**) were determined using single-crystal X-ray crystallography. Theoretical calculations based on density functional theory were performed using the full crystal structures of **1**, **2**, $[Cu_3(PhPyCNO)_3(OH)(CH_3OH)_2(ClO_4)_2]$ (**3**), and $[Cu_3(PhPyCNO)_3(\mu_3\text{-}OMe)(Cl)(ClO_4)]$ (**4**). The geometries of the model compounds $[Cu_3(\kappa^3N,N,O\text{-}HNCHCHNO)_3(\mu_3\text{-}OH)(\mu_2\text{-}HCOO)(HCOO)]$ (**5**), $[Cu_3(\kappa^3N,N,O\text{-}HNCHCHNO)_3(\mu_2\text{-}HCOO)(HCOO)]^+$ (**6**), $[Cu_3(\kappa^3N,N,O\text{-}HNCHCHNO)_3(\mu_3\text{-}O)]^+$ (**7**), and $[Cu_3(\kappa^3N,N,O\text{-}HNCHCHNO)_3]^{3+}$ (**8**) were optimized at the same level of theory for both the doublet and quartet states, and vibrational analysis indicated that the resulting equilibrium geometries corresponded to minima on the potential energy surfaces. Both e_g and t_{2g} magnetic orbitals seem to contribute to the magnetic exchange coupling. The latter contribution, although less important, might be due to overlap of the t_{2g} orbitals with the p-type orbitals of the central triply bridging oxide ligand, thereby affecting its displacement from the Cu_3 plane and contributing to the antiferromagnetic coupling. The crucial role of the triply bridging oxide (μ_3-O) ligand on the antiferromagnetic exchange coupling between the three Cu(II) magnetic centers is further evidenced by the excellent linear correlation of the coupling constant *J* with the distance of the μ_3-O ligand from the centroid of the Cu_3 triangle.

Introduction

It has been remarked that the attention of coordination chemists is increasingly directed to polynuclear systems. Metallacrowns (MCs),[1] the inorganic structural and functional analogues of crown ethers, are usually formed with transition-metal ions and a nitrogen replacing the methylene carbons. MCs exhibit selective recognition of cations and anions, and these complexes can display intramolecular magnetic exchange interactions.[1,2] There is also a renewed interest in the coordination chemistry of oximes. These research efforts are being driven by a number of

* Corresponding authors. E-mail: vtango@upatras.gr (V.T.), attsipis@uoi.gr (A.T.), kessisog@chem.auth.gr (D.P.K.).
[†] Aristotle University of Thessaloniki.
[‡] NCSR "Demokritos".
[||] University of Ioannina.

(1) (a) Mezei, G.; Zaleski, C. M.; Pecoraro, V. L. *Chem. Rev.* **2007**, *107*, 4933–5003. (b) Pecoraro, V. L.; Stemmler, A. J.; Gibney, B. R.; Bodwin, J. J.; Wang, H.; Kampf, J. W.; Barwinski, A. *Prog. Inorg. Chem.* **1997**, *45*, 83–177.

10.1021/ic8003257 CCC: $40.75
Published on Web 08/06/2008

considerations, including the solution of pure chemical problems, the development of new oxygen activation catalysts, and the employment of oximate ligands in the synthesis of homometallic or heterometallic complexes having interesting magnetic properties such as single-molecule magnetism.[3]

Two structural motifs in 9-MC-3 metallacrowns have been reported: regular and inverse.[2p,3a,b] In the regular motif, the metallacrown ring shows the repeating pattern [−O−N−M−] with the oxygen atoms oriented toward the center of the cavity. In the inverse motif, the repeating [−O−N−M−] pattern remains the same, but the metal atoms are oriented toward the center of the cavity. Regular metallacrowns bind cations in a central cavity, while inverse metallacrowns can bind anions.

The majority of inverse metallacrowns reported previously have been prepared using di-2-pyridyl ketoxime (Hpko) as the constructing ligand. Hpko is a bifunctional ligand that can bind metals in either five- or six-membered chelate rings, and the structures reported to date show that the Hpko ligand possesses a considerable variety of coordination modes (Scheme 1).

Scheme 1. Coordination Modes Observed for Binding of the Hpko$^-$ Ligand with Copper, Labeled Using the Harris Notation[4f]

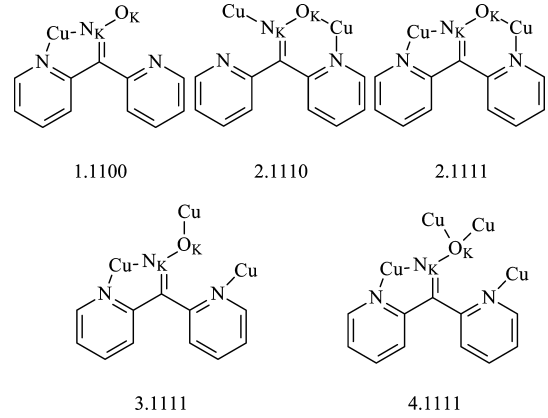

Interest in the synthesis of polynuclear (especially trinuclear) copper complexes and studies of their physical and chemical properties stems from the recent knowledge that a trinuclear array of copper(II) centers may be the essential functional unit in a number of multicopper blue oxidases,[4] such as laccase and ascorbate oxidases. In addition, there is a clear interest in cyclic trinuclear copper complexes,[5] since these systems can be regarded as geometrically frustrated and therefore offer the opportunity to test magnetic exchange models.

Our previous efforts have been centered on the preparation and characterization of trinuclear Cu(II) inverse-metallacrown compounds in order to understand the magnetochemistry in these types of complexes.[3a,b]

In this article, we report the crystal structure of two compounds, $[Cu_3(PhPyCNO)_3(\mu_3\text{-}OH)(2,4,5\text{-}T)_2]$ (**1**), where 2,4,5-T is 2,4,5-trichlorophenoxyacetate, and $[Cu_3(PhPyCNO)_3(\mu_3\text{-}OH)(H_2O)(ClO_4)_2]$ (**2**), which were obtained using phenyl 2-pyridyl ketoxime (PhPyCNOH) as the constructing ligand. We also report the results of experimental and theoretical magnetic studies of the series of *inverse*-9-MC-3 metallacrowns **1**, **2**, $[Cu_3(PhPyCNO)_3(OH)(CH_3OH)_2(ClO_4)_2]$ (**3**),[3b] and $[Cu_3(PhPyCNO)_3(\mu_3\text{-}OMe)(Cl)(ClO_4)]$ (**4**)[3b] and of the model complexes $Cu_3(\kappa^3N,N,O\text{-}HNCHCHNO)_3(\mu_3\text{-}O)(\mu_2\text{-}HCOO)(HCOO)]$ (**5**), $Cu_3(\kappa^3N,N,O\text{-}HNCHCHNO)_3(\mu_2\text{-}HCOO)(HCOO)]^+$ (**6**), $Cu_3(\kappa^3N,N,O\text{-}HNCHCHNO)_3(\mu_3\text{-}O)]^+$ (**7**), and $Cu_3(\kappa^3N,N,O\text{-}HNCHCHNO)_3]^{3+}$ (**8**), which were performed in order to explore the magnetic behavior of these types of copper complexes.

Experimental Section

Caution! *Although no problems in handling perchlorate compounds were experienced in the present work, these salts are potentially explosive when combined with organic ligands and should be manipulated with care and used only in small quantities.*

(2) (a) Dendrinou-Samara, C.; Alexiou, M.; Zaleski, C. J.; Kampf, J. W.; Kirk, M. L.; Kessissoglou, D. P.; Pecoraro, V. L. *Angew. Chem, Int. Ed.* **2003**, *42*, 3763–3766. (b) Zaleski, C. J.; Depperman, E.; Kampf, J. W.; Kirk, M. L.; Pecoraro, V. L. *Angew. Chem., Int. Ed.* **2004**, *43*, 3912–3914. (c) Dendrinou-Samara, C.; Alexiou, M.; Zaleski, C. J.; Kampf, J. W.; Depperman, E.; Kessissoglou, D. P.; Kirk, M. L.; Pecoraro, V. L. *J. Am. Chem. Soc.* **2005**, *127*, 12862–12872. (d) Zaleski, C. J.; Depperman, E.; Kampf, J. W.; Kirk, M. L.; Pecoraro, V. L. *Inorg. Chem.* **2006**, *45*, 10022–10024. (e) Bodwin, J. J.; Cutland, A. D.; Malkani, R. G.; Pecoraro, V. L. *Coord. Chem. Rev.* **2001**, *216*−*217*, 489–512. (f) Dendrinou-Samara, C.; Zaleski, C. M.; Evagorou, A.; Kampf, J. W.; Pecoraro, V. L.; Kessissoglou, D. P. *Chem. Commun.* **2003**, 2668–2669. (g) Psomas, G.; Stemmler, A. J.; Dendrinou-Samara, C.; Bodwin, J. J.; Schneider, M.; Alexiou, M.; Kampf, J. W.; Kessissoglou, D. P.; Pecoraro, V. L. *Inorg. Chem.* **2001**, *40*, 1562–1570. (h) Dendrinou-Samara, C.; Psomas, G.; Iordanidis, L.; Tangoulis, V.; Kessissoglou, D. P. *Chem.*−*Eur. J.* **2001**, *7*, 5041–5051. (i) Dendrinou-Samara, C.; Alevizopoulou, L.; Iordanidis, L.; Samaras, E.; Kessissoglou, D. P. *J. Inorg. Biochem.* **2002**, *89*, 89–96. (j) Cutland, A. D.; Halfen, J. A.; Kampf, J. W.; Pecoraro, V. L. *J. Am. Chem. Soc.* **2001**, *123*, 6211–6212. (k) Stemmler, A. J.; Kampf, J. W.; Kirk, M. L.; Atasi, B. H.; Pecoraro, V. L. *Inorg. Chem.* **1999**, *38*, 2807–2817. (l) Psomas, G.; Dendrinou-Samara, C.; Alexiou, M.; Tsohos, A.; Raptopoulou, C. P.; Terzis, A.; Kessissoglou, D. P. *Inorg. Chem.* **1998**, *37*, 6556–6557. (m) Alexiou, M.; Dendrinou-Samara, C.; Raptopoulou, C. P.; Terzis, A.; Kessissoglou, D. P. *Inorg. Chem.* **2002**, *41*, 4732–4738. (n) Alexiou, M.; Dendrinou-Samara, C.; Raptopoulou, C. P.; Terzis, A.; Tangoulis, V.; Kessissoglou, D. P. *Eur. J. Inorg. Chem.* **2004**, 3822–3827. (o) Dendrinou-Samara, C.; Alexiou, M.; Zaleski, C. M.; Kampf, J. W.; Kirk, M. L.; Kessissoglou, D. P.; Pecoraro, V. L. *Angew. Chem., Int. Ed.* **2003**, *42*, 3763–3766. (p) Alexiou, M.; Katsoulakou, E.; Dendrinou-Samara, C.; Raptopoulou, C. P.; Psycharis, V.; Manessi-Zoupa, E.; Perlepes, S. P.; Kessissoglou, D. P. *Eur. J. Inorg. Chem.* **2005**, 1964–1978.

(3) (a) Afrati, T.; Zaleski, C. M.; Dendrinou-Samara, C.; Mezei, G.; Kampf, J. W.; Pecoraro, V. L.; Kessissoglou, D. P. *Dalton Trans.* **2007**, 2658–2668. (b) Afrati, T.; Dendrinou-Samara, C.; Raptopoulou, C.; Terzis, A.; Tangoulis, V.; Kessissoglou, D. P. *Dalton Trans.* **2007**, 5156–5164. (c) Milios, C. J.; Stamatatos, C.; Kyritsis, P.; Terzis, A.; Raptopoulou, C. P.; Vicente, R.; Escuer, A.; Perlepes, S. P. *Eur. J. Inorg. Chem.* **2004**, 2885–2901. (d) Chaudhuri, P. *Coord. Chem. Rev.* **2003**, *243*, 143–190. (e) Kukushkin, V. Y.; Pombeiro, A. J. L. *Coord. Chem. Rev.* **1999**, *181*, 147–175. (f) Kukushkin, V. Y.; Tudela, D.; Pombeiro, A. J. L. *Coord. Chem. Rev.* **1996**, *156*, 333–362. (g) Milios, C. J.; Kyritsis, P.; Raptopoulou, C. P.; Terzis, A.; Vicente, R.; Escuer, A.; Perlepes, S. P. *Dalton Trans.* **2005**, 501–511. (j) Stamatatos, T. C.; Vlahopoulou, J. C.; Sanakis, Y.; Raptopoulou, C. P.; Psycharis, V.; Boudalis, A. K.; Perlepes, S. P. *Inorg. Chem. Commun.* **2006**, *9*, 814–818.

(4) (a) Solomon, E. I.; Tuczek, F.; Root, D. E.; Brow, C. A. *Chem. Rev.* **1994**, *94*, 827–856. (b) Isele, K.; Franz, P.; Ambrus, C.; Bernardinelli, G.; Decurtins, S.; Williams, A. F. *Inorg. Chem.* **2005**, *44*, 3896–3906. (c) Jiang, Y.-B.; Kou, H.-Z.; Wang, R.-J.; Cui, A.-L.; Ribas, J. *Inorg. Chem.* **2005**, *44*, 709–715. (d) Yoon, J.; Mirica, L. M.; Stack, T. D. P.; Solomon, E. I. *J. Am. Chem. Soc.* **2005**, *127*, 13680–13693. (e) Messerschmidt, A. *Struct. Bonding (Berlin)* **1998**, *90*, 37–68. (f) Coxall, R. A.; Harris, S. G.; Henderson, D. K.; Parsons, S.; Tasker, P. A.; Winpenny, R. E. P. *J. Chem. Soc., Dalton Trans.* **2000**, *90*, 2349–2356.

Table 1. Crystal Data and Structure Refinement Parameters for **1** and **2**

	1	**2**
empirical formula	$C_{53.80}H_{43.20}Cl_6Cu_3N_6O_{11.80}$	$C_{36}H_{30}Cl_2Cu_3N_6O_{13}$
formula weight	1365.86	1016.18
T (K)	298	298
crystal system	monoclinic	monoclinic
space group	$P2_1/n$	$C2/c$
a (Å)	18.140(9)	37.57(3)
b (Å)	14.009(7)	7.956(6)
c (Å)	23.087(10)	29.53(2)
α (deg)	90.00	90
β (deg)	102.76(2)	115.67(2)
γ (deg)	90.00	90
V (Å^3)	5722(5)	7956(10)
Z	4	8
D_{calcd} (Mg m^{-3})	1.585	1.697
absorption coefficient (mm^{-1})	4.428	1.797
F(000)	2766	4104
θ range for data collection	3.72−57.34°	2.22−24.25°
index ranges	$-19 \le h \le 18$, $0 \le k \le 15$, $0 \le l \le 25$	$-43 \le h \le 0$, $-9 \le k \le 0$, $-30 \le l \le 33$
goodness of fit on F^2	1.026	1.098
final R indices R1, wR2 [$I > 2\sigma(I)$]	0.0557, 0.1341[a]	0.0513, 0.1153[b]

[a] For 5329 reflections with $I > 2\sigma(I)$. [b] For 4501 reflections with $I > 2\sigma(I)$.

Materials. *N,N*-Dimethylformamide (DMF) distilled from CaH_2 and methanol distilled from Mg were stored over 3 Å molecular sieves. $Cu(ClO_4)_2 \cdot 6H_2O$, $CuCl_2 \cdot 2H_2O$, phenyl 2-pyridyl ketoxime, and 2,4,5-trichlorophenoxyacetic acid (2,4,5-TH) were purchased from Aldrich and used as received. All of the chemicals and solvents were reagent-grade.

Preparation of $[Cu_3(PhPyCNO)_3(\mu_3\text{-}OH)(2,4,5\text{-}T)_2] \cdot 1.8CH_3OH$ (1). The complex was synthesized by adding 0.6 mmol (0.12 g) of phenyl 2-pyridyl ketoxime to 0.6 mmol (0.1 g) of $CuCl_2 \cdot 2H_2O$ in 30 mL of methanol following the addition of 0.4 mmol (0.09 g) of 2,4,5-TH and 1.2 mmol (0.05 g) of NaOH. The volume of the resulting dark-green solution was reduced to 10 mL after 5 h of stirring. The solution was left to slowly evaporate, and after 3 days, dark-green crystals were deposited from the mother liquor. These crystals were structurally characterized and found to have the formula $C_{53.80}H_{43.20}Cl_6Cu_3N_6O_{11.80}$ (fw 1365.86). Anal. Calcd: C, 47.26; H, 3.16; N, 6.14. Found: C, 47.40; H, 3.00; N, 6.30. Yield: 65%.

Preparation of $[Cu_3(PhPyCNO)_3(OH)(H_2O)(ClO_4)_2]$ (2). The complex was synthesized by dissolving 1 mmol (0.37 g) of $Cu(ClO_4)_2 \cdot 6H_2O$, 1 mmol (0.2 g) of phenyl 2-pyridyl ketoxime, and 1 mmol (0.04 g) of NaOH in 20 mL of methanol. The volume of the resulting dark-green solution was reduced to 10 mL after 5 h of stirring. The solution was left to slowly evaporate, and after 1 day, dark-green crystals were deposited from the mother liquor. These crystals were structurally characterized and found to have the formula $C_{36}H_{30}Cl_2Cu_3N_6O_{13}$ (fw 1016.18). Anal. Calcd: C, 42.51; H, 2.95; N, 8.26. Found: C, 42.50; H, 3.00; N, 8.50. Yield: 50%.

Physical Measurements. Infrared (IR) spectra (200−4000 cm^{-1}) were recorded on a Perkin-Elmer FT-IR 1650 spectrometer using samples prepared as KBr pellets. UV−vis spectra were recorded on a Shimadzu-160A dual-beam spectrophotometer. Room-temperature magnetic measurements were carried out using Faraday's method with mercury tetrathiocyanatocobaltate(II) as the calibrant. Variable-temperature magnetic susceptibility measurements were carried out on powdered samples over the temperature range 3−300 K using a Quantum Design SQUID susceptometer in applied magnetic fields of 0.1 and 1.0 kG. Magnetization measurements were carried out at various temperatures in the range 1.8−6 K over the field range 0−5 T. Elemental analyses for C, H, and N were performed on a Perkin-Elmer 240B elemental analyzer. Electric conductance measurements were carried out using a WTW model LF 530 conductivity outfit and a type-C cell having a cell constant of 0.996 (representing a mean value calibrated at 25 °C with potassium chloride). All of the temperatures were controlled within an accuracy of ±0.1 °C using a Haake thermoelectric circulating system.

Structure Determination. A dark-green, parallelepipedal crystal of **1** having approximate dimensions 0.08 × 0.18 × 0.75 mm and a dark-green crystal of **2** having approximate dimensions 0.10 × 0.40 × 0.70 mm were mounted in capillaries. Diffraction measurements were made on a $P2_1$ Nicolet diffractometer upgraded by Crystal Logic (for **1**) and on a Crystal Logic Dual Goniometer (for **2**) using graphite-monochromatized Cu Kα and Mo Kα radiation for **1** and **2**, respectively. Crystal data and data collection parameters are reported in Table 1.

Unit-cell dimensions were determined and refined using the angular settings of 25 automatically centered reflections in the ranges $22° < 2\theta < 54°$ and $11° < 2\theta < 23°$ for **1** and **2**, respectively. Intensity data were recorded using $\theta-2\theta$ scans. Three standard reflections monitored every 97 reflections showed intensity fluctuations of <3.0% and no decay. Lorentz, polarization, and ψ-scan absorption corrections were applied using Crystal Logic software. The structures of **1** and **2** were solved by direct methods using the program SHELXS-97[6] and refined by full-matrix least-squares techniques on F^2 using SHELXL-97.[7]

Additional crystallographic details for **1**: $2\theta = 114.5°$; scan speed = 1.5 deg min^{-1}; scan range = 2.45° + $\alpha_1\alpha_2$ separation; no. of reflections collected, unique [R(int)], used = 8399, 7683 [0.0534], 7683; no. of parameters refined = 878; R1, wR2 (all data) = 0.0904, 0.1592; $[\Delta/\sigma]_{max} = 0.003$. All of the hydrogen atoms were located using difference maps and refined isotropically except for those of the solvate methanol molecules, which were introduced at calculated positions as riding on bonded atoms. All of the non-hydrogen atoms were refined anisotropically.

Additional crystallographic details for **2**: $2\theta = 48.5°$; scan speed = 1.5 deg min^{-1}; scan range = 1.6° + $\alpha_1\alpha_2$ separation; no. of reflections collected, unique [R(int)], used = 6373, 6267 [0.0348], 6267; no, of parameters refined = 661; R1, wR2 (all data) = 0.0854, 0.1343; $[\Delta/\sigma]_{max} = 0.004$. All of the hydrogen atoms were located using difference maps and refined isotropically. All of the non-hydrogen atoms were refined anisotropically.

The supplementary crystallographic data for compounds **1** and **2** were deposited with the Cambridge Crystallographic Data Centre (CCDC) (nos. 678392 and 678393, respectively). These data can be obtained free of charge at www.ccdc.cam.ac.uk/conts/retrieving.html or from the CCDC, 12 Union Road, Cambridge CB2 1EZ, U.K. [fax, (+44) 1223−336−033; e-mail, deposit@ccde.cam.ac.uk].

Results and Discussion

Preparation of complexes **1** and **2** was achieved by reaction of $CuCl_2$ and $Cu(ClO_4)_2$, respectively, with $PhPyCNO^-$ in MeOH solution at room temperature in the presence and absence, respectively, of the alkanoato sodium salt 2,4,5-T (eqs 1 and 2, respectively):

$$3CuCl_2 + 3PhPyCNOH + 6NaOH + 2Cl_3C_6H_2OCH_2COOH \xrightarrow{MeOH} [Cu_3(PhPyCNO)_3(OH)(Cl_3C_6H_2OCH_2COO)_2] + 6NaCl + 5H_2O \quad (1)$$

$$3Cu(ClO_4)_2 + 3PhPyCNOH + 4NaOH \xrightarrow{MeOH} [Cu_3(PhPyCNO)_3(OH)(H_2O)(ClO_4)_2] + 4NaClO_4 + 2H_2O \quad (2)$$

The dark-green crystals are soluble in dmf and dmso, with **1** being a nonelectrolyte and **2** a 1:2 electrolyte in these solvents. The IR spectrum of **1** exhibited bands characteristic of the ligand $PhPyCNO^-$ [ν (cm^{-1}) 1598 (s, pyridyl C═N), 1465 (vs, N−O)]. Tentative assignments of the IR bands for the asymmetric [$\nu_{asym}(CO_2)$] and symmetric [$\nu_{sym}(CO_2)$] stretching vibrations as well as the difference $\Delta = \nu_{asym}(CO_2) - \nu_{sym}(CO_2)$, which are useful characteristics for determining the coordination mode of carboxylato ligands, were the following for **1**: a strong doublet band (1611 and 1584 cm^{-1}) was attributed to $\nu_{asym}(CO_2)$, and a strong doublet band (1410 and 1363 cm^{-1}) was attributed to $\nu_{sym}(CO_2)$. The calculated Δ values suggested more than one coordination mode of the carboxylato ligands. On the basis of the crystal structure of **1**, the values of 174 and 221 cm^{-1} for Δ were excluded, while the Δ values of 140 and 248 cm^{-1}, suggesting bidentate bridging and unidentate coordination modes, respectively, were considered to be more realistic. The IR spectrum of **2** confirmed the presence of the $PhPyCNO^-$ ligand by exhibiting the same characteristic bands [ν (cm^{-1}) 1596 (s, pyridyl C═N), 1464 (vs, N−O)], and the perchlorate anion bands at 1103 (vs, br), 1031 (m), and 623 cm^{-1} (s) [assigned to the $\nu(Cl-O)_{asym}$, $\nu(Cl-O)_{sym}$, and $\delta(Cl-O)$ vibrations, respectively] were not diagnostic for the coordination mode of the ligand.

Table 2. Selected Bond Distances and Angles in **1**

Bond Distances (Å)			
Cu1−O11	1.925(4)	Cu2−O41	2.239(4)
Cu1−N2	1.968(5)	Cu2−O51	1.953(4)
Cu1−N1	1.974(5)	Cu3−N21	1.957(5)
Cu1−O31	2.198(5)	Cu3−O51	1.920(5)
Cu1−O51	1.953(4)	Cu3−O1	1.934(4)
Cu2−O21	1.971(4)	Cu3−N22	1.981(5)
Cu2−N12	1.986(5)	Cu3−O32	2.326(5)
Cu2−N11	1.988(5)		
Bond Angles (deg)			
O11−Cu1−N2	175.9(2)	N12−Cu2−O41	94.6(2)
O11−Cu1−O31	93.4(2)	O51−Cu3−N21	166.4(2)
N2−Cu1−O31	89.4(2)	O1−Cu3−N22	173.3(2)
N1−Cu1−O31	93.9(2)	O51−Cu3−O32	89.4(2)
O51−Cu1−O31	99.6(2)	O1−Cu3−O32	101.0(2)
O51−Cu1−N1	163.3(2)	N21−Cu3−O32	100.9(2)
O21−Cu2−N12	168.8(2)	N22−Cu3−O32	83.7(2)
O51−Cu2−N11	162.2(2)	Cu3−O51−Cu2	109.0(2)
O51−Cu2−O41	92.6(2)	Cu3−O51−Cu1	108.0(2)
N11−Cu2−O41	102.3(2)	Cu2−O51−Cu1	110.5(2)
O21−Cu2−O41	96.4(2)		

Crystal Structures. Selected bond distances and angles for complexes **1** and **2** are listed in Tables 2 and 3, respectively.

Description of the Structure of 1. The structure of **1** consists of a triangular $[Cu_3(PhPyCNO)_3(\mu_3\text{-}OH)(2,4,5\text{-}T)_2]$ unit (Figure 1). The geometry around each of the copper(II) ions in the trimeric unit is best described as a distorted square pyramid having a NNOOO coordination environment. The trimeric skeleton is created by the oximato nitrogen atoms of one $PhPyCNO^-$ ligand and the oxime oxygen atom of the adjacent $PhPyCNO^-$ligand, while the O atom of the μ_3-OH^- ligand (O51) completes the square-planar bases of the three metal atoms, with Cu1−O51, Cu2−O51, and Cu3−O51 bond distances of 1.954(5), 1.953(4), and 1.919(5) Å, respectively. The two alkanoato 2,4,5-T ligands are bound to opposite sides of the trimeric unit, one in bidentate and the other in monodentate mode. The bidentate alkanoato ligand bridges Cu1 and Cu3, with Cu1−O31 and Cu3−O32 distances of 2.198(5) and 2.323(6) Å, respectively, while the oxygen of the monodentate ligand occupies the apical

(5) (a) Spiccia, L.; Graham, B.; Hearn, M. T. W.; Lazarev, G.; Moubaraki, B.; Murray, K. S.; Tiekink, E. D. *J. Chem. Soc., Dalton Trans.* **1997**, 4089–4098. (b) Winpenny, R. E. P. *Adv. Inorg. Chem.* **2001**, *52*, 1. (c) Ferrer, S.; Haasnoot, J. G.; Reedijk, J.; Müller, E.; Biagini Cingi, M.; Lanfranchi, M.; Manotti Lanfredi, A. M.; Ribas, J. *Inorg. Chem.* **2000**, *39*, 1859–1867. (d) Sakai, K.; Yamada, Y.; Tsubomura, T.; Yabuki, M.; Yamaguchi, M. *Inorg. Chem.* **1996**, *35*, 542–544. (e) Blake, A. B.; Sinn, E.; Yavari, A.; Murray, K. S.; Moubaraki, B. *J. Chem. Soc., Dalton Trans.* **1998**, 45–50. (f) Angaroni, M.; Ardizzoia, G. A.; Beringhelli, T.; La Monica, G.; Gatteschi, D.; Masciocchi, N.; Moret, M. *J. Chem. Soc., Dalton Trans.* **1990**, 3305–3309. (g) Isele, K.; Franz, P.; Ambrus, C.; Bernardinelli, G.; Decurtins, S.; Williams, A. F. *Inorg. Chem.* **2005**, *44*, 3896–3906. (h) Bailey, N. A.; Fenton, D. E.; Moody, R.; Scrimshire, P. J.; Beloritzky, E.; Fries, P. H.; Latour, J.-M. *J. Chem. Soc., Dalton Trans.* **1988**, 2817–2824. (i) Curtis, N. F.; Gladkikh, O. P.; Heath, S. L.; Morgan, K. R. *Aust. J. Chem.* **2000**, *53*, 577–582. (j) Larionov, S. V.; Myachina, L. I.; Romanenko, G. V.; Tkachev, A. V.; Seludyakova, L. A.; Ikorskii, V. N.; Boguslavskii, E. G. *Russ. J. Coord. Chem.* **2001**, *27*, 455–464. (k) Abedin, T. S. M.; Thompson, L. K.; Mille, D. O.; Krupicka, E. *Chem. Commun.* **2003**, 708–709. (l) Cabeza, J. A.; del Rio, I.; Rieva, V.; Suárez, M.; Alvarez-Rúa, C.; Garcia-Granda, S.; Chuang, S. H.; Hwu, J. R. *Eur. J. Inorg. Chem.* **2003**, 4159–4165. (m) Mirica, L. M.; Stack, T. D. P.; Solomon, E. I. *J. Am. Chem. Soc.* **2004**, *126*, 12586–12595. (n) Mirica, L. M.; Stack, T. D. P. *Inorg. Chem.* **2005**, *44*, 2131–2133. (o) Yoon, J.; Mirica, L. M.; Stack, T. D. P.; Solomon, E. I. *J. Am. Chem. Soc.* **2005**, *127*, 13680–13693. (p) Yoon, J.; Solomon, E. I. *Coord. Chem. Rev.* **2007**, *251*, 379–400. (q) Yoon, J.; Solomon, E. I. *Inorg. Chem.* **2005**, *44*, 8076–8086. (r) Ferrer, S.; Lloret, F.; Bertomeu, I.; Alzuet, G.; Borrás, J.; García-Granda, S.; Liu-González, M.; Haasnoot, J. G. *Inorg. Chem.* **2002**, *41*, 5821–5830. (s) López-Sandoval, H.; Contreras, R.; Escuer, A.; Vicente, R.; Bernès, S.; Nöth, H.; Leigh, G. J.; Barba-Behrens, N. *J. Chem. Soc., Dalton Trans.* **2002**, 2648–2653. (t) Liu, X.; de Miranda, M. P.; McInnes, E. J. L.; Kilner, C. A.; Halcrow, M. A. *Dalton Trans.* **2004**, 59–64.

(6) Sheldrick, G. M. *SHELXS-97, Crystal Structure Solving Program*; University of Göttingen: Göttingen, Germany, 1997.

(7) Sheldrick, G. M. *SHELXL-97, Crystal Structure Refinement Program*; University of Göttingen: Göttingen, Germany, 1997.

Table 3. Selected Bond Distances and Angles in **2**

Bond Distances (Å)			
Cu1−O51	2.474(4)	Cu2−N12	1.966(5)
Cu1−O31	1.949(4)	Cu2−Ow	2.421(8)
Cu1−N1	1.964(5)	Cu3−Ow	2.695(8)
Cu1−N2	1.969(5)	Cu3−O1	1.912(4)
Cu1−O11	1.923(4)	Cu3−O31	1.979(5)
Cu2−O31	1.964(5)	Cu3−N21	1.974(5)
Cu2−N11	1.982(5)	Cu3−N22	1.968(5)
Cu2−O21	1.921(4)	Cu3−O41	2.550(5)
Cl1−O44	1.420(6)	Cl2−O53	1.355(8)
Cl1−O43	1.427(6)	Cl2−O52	1.37(1)
Cl1−O42	1.413(5)	Cl2−O54	1.333(8)
Cl1−O41	1.438(5)	Cl2−O51	1.350(6)
Bond Angles (deg)			
O11−Cu1−O31	94.0(2)	N11−Cu2−N12	80.8(2)
O11−Cu1−N1	93.2(2)	O21−Cu2−Ow	90.7(2)
O31−Cu1−N1	172.2(2)	O31−Cu2−Ow	76.9(3)
O11−Cu1−N2	161.6(2)	N11−Cu2−Ow	109.1(3)
O31−Cu1−N2	91.2(2)	N12−Cu2−Ow	91.1(2)
N1−Cu1−N2	81.0(2)	O1−Cu3−O31	94.2(2)
O21−Cu2−O31	94.4(2)	O1−Cu3−N21	94.7(2)
O21−Cu2−N11	94.7(2)	O31−Cu3−N21	168.5(2)
O31−Cu2−N11	169.1(2)	O1−Cu3−N22	173.4(2)
O21−Cu2−N12	175.5(2)	O31−Cu3−N22	90.2(2)
O31−Cu2−N12	90.1(2)	N21−Cu3−N22	81.6(2)

position of the Jahn−Teller-elongated square pyramid of Cu2, with a Cu2−O41 distance of 2.239(4) Å.

Each set of four atoms defining one of the basal planes around the Cu(II) ions deviates slightly from planarity, with torsion angles of 168.911 and 168.949° for the Cu1 plane, 175.640 and 175.664° for the Cu3 plane, and 160.174 and 160.441° for the Cu2 plane; the copper atoms lie on the square basal planes, with the sums of the angles around the copper atoms being 359.29, 357.15, and 359.15° for Cu1 for Cu2, and Cu3, respectively. The Cu_3 unit can be considered as an equilateral triangle with Cu1···Cu3, Cu2···Cu3, and Cu1···Cu2 distances of 3.135, 3.153, and 3.210 Å, respectively.

The *inverse*-9-$MC_{Cu(II)(PhPyCNO)}$-3 ring is almost planar, with torsion angles varying between 170 and 179°. The oxygen atom of the hydroxy ligand, which is trapped in the metallacrown ring, lies a distance of 0.66 Å out of the plane defined by the copper atoms.

Description of the Structure of 2. The structure of **2** consists of a triangular $[Cu_3(PhPyCNO)_3(\mu_3\text{-}OH)(H_2O)(ClO_4)_2]$ unit (Figure 2). The geometry around Cu3 in the trimeric unit is best described as a distorted octahedron having a N_2O_4 coordination environment, while the other two copper(II) ions have square-pyramidal N_2O_3 environments. The trimeric skeleton is created by the oximato nitrogen atoms of one $PhPyCNO^-$ ligand and the oxime oxygen atom of the adjacent $PhPyCNO^-$ligand, while the O atom of the μ_3-OH^- ligand (O31) completes square-planar bases of the three metal atoms, with Cu1−O31, Cu2−O31, and Cu3−O31 bond distances of 1.949(4), 1.964(4), and 1.979(5) Å, respectively. The μ-H_2O ligand caps the opposite side of Cu_3 plane, occupying the apical positions of the coordination spheres of Cu2 and Cu3, with Cu2−Ow and Cu3−Ow bond distances of 2.421(8) and 2.695(8) Å, respectively. The sums of four angles around the three Cu(II) atoms are 359.4, 359.97, and 360.69° for Cu1, Cu2, and Cu3, respectively, showing that all of the Cu(II) atoms lie on the square basal planes. A terminal ClO_4^- ion completes the octahedral geometry around Cu3, with a Cu3−O41 bond distance of 2.550(5) Å, and another terminal ClO_4^- ion occupies the apical position of the Jahn−Teller-distorted square pyramid of Cu1, with a Cu1−O51 bond distance of 2.474(4) Å. The Cu_3 cluster can be considered as an equilateral triangle, with Cu1···Cu2, Cu2···Cu3, and Cu1···Cu3 distances of 3.208, 3.136, and 3.220 Å, respectively. The *inverse*-9-$MC_{Cu(II)(PhPyCNO)}$-3 ring is almost planar, with the torsion angles between the Cu_3 plane and the oxygen or nitrogen atoms constructing the metallacrown ring having deviations from planarity of 2−11°. The oxygen atom of the hydroxy ligand trapped in the metallacrown ring lies a distance of 0.68 Å out of the plane defined by the copper atoms, and the water oxygen lies 1.98 Å out of the Cu_3 plane.

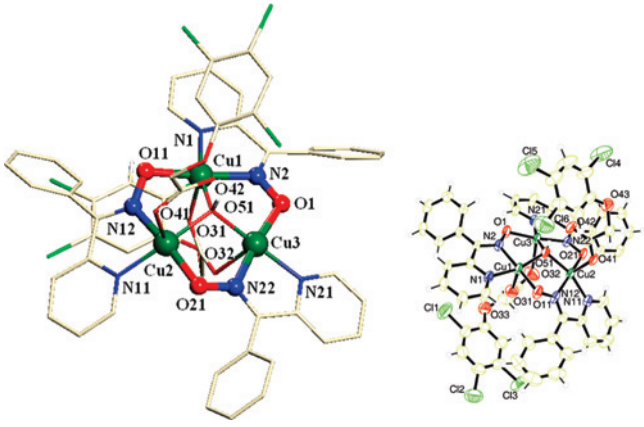

Figure 1. (left) X-ray crystal structure of **1** and (right) an ORTEP diagram of **1** using 50% ellipsoids; all of the heteroatoms are labeled.

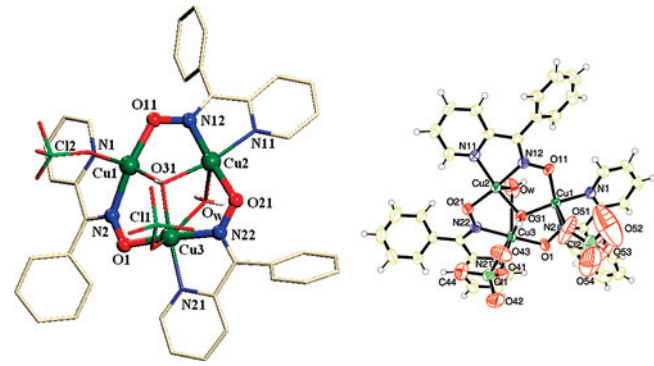

Figure 2. (left) X-ray crystal structure of **2** and (right) an ORTEP diagram of **2** using 50% ellipsoids; all of the heteroatoms are labeled.

Magnetic Susceptibility Measurements on 1. The temperature dependence of the magnetic susceptibility of **1** is shown in Figure 3 as a plot of $\chi_M T$ versus T. The $\chi_M T$ data decrease drastically, from the room-temperature value of ~0.67 emu mol^{-1} K, which is smaller than the value of 1.125 emu mol^{-1} K expected for three independent Cu(II) ions, to a value of 0.29 emu mol^{-1} K at 2 K.

The isotropic Heisenberg−Dirac−van Vleck (HDvV) Hamiltonian (eq 3) was the main term used to interpret the magnetic data:

$$\hat{H} = -2J_{12}\hat{\mathbf{S}}_1\cdot\hat{\mathbf{S}}_2 - 2J_{13}\hat{\mathbf{S}}_1\cdot\hat{\mathbf{S}}_3 - 2J_{23}\hat{\mathbf{S}}_2\cdot\hat{\mathbf{S}}_3 \quad (3)$$

The distances between the magnetic ions in complex **1** are almost equal, which would imply that the three J_{ij} constants are equal. When we assumed that the three J_{ij} values were equal, the data were reproduced reasonably well, and values of -220 cm^{-1}, 2.10(1), and 120×10^{-6} cm^3 mol^{-1} for J_{ij}, g, and the temperature-independent paramagnetism (TIP), respectively, were obtained. The quality of the magnetic susceptibility data did not vary significantly when we assumed an isosceles-triangle structure ($J_{12} = J_{13} \neq J_{23}$). The resolution of our data in the high-temperature range, however, did not allow us to accurately determine the difference $|J_{12} - J_{23}|$. However, there is an obvious discrepancy concerning magnetic susceptibility between the magnetic model and the experimental results at low temperatures (Figure 3). In order to clarify the low-temperature behavior, systematic measurements of the susceptibility data were carried out at different magnetic fields, and the results are shown in Figure 4.

It is well documented that the antisymmetric exchange interaction plays an important role in the magnetic behavior of the system, so a new magnetic model that also includes this kind of interaction (eq 4) was used:

$$H = -2J_0(\hat{\mathbf{S}}_1\cdot\hat{\mathbf{S}}_2 + \hat{\mathbf{S}}_1\cdot\hat{\mathbf{S}}_3) - 2J_1\hat{\mathbf{S}}_2\cdot\hat{\mathbf{S}}_3 + \mathbf{G}\cdot([\hat{\mathbf{S}}_1\times\hat{\mathbf{S}}_2] + [\hat{\mathbf{S}}_2\times\hat{\mathbf{S}}_3] + [\hat{\mathbf{S}}_3\times\hat{\mathbf{S}}_1]) + (g_z\cos\theta + g_{xy}\sin\theta)\beta\mathbf{H}\cdot(\hat{\mathbf{S}}_1 + \hat{\mathbf{S}}_2 + \hat{\mathbf{S}}_3) \quad (4)$$

where J_0 and J_1 are the isotropic exchange interactions (which differ because of the symmetry reduction), **H** is the magnetic field vector, and **G** is the antisymmetric exchange vector parameter[8] for a two-center interaction, which has been described in a previous report.[3b] In trigonal systems, the components of **G** are assumed to follow the relation $G_z \gg (G_x, G_y) \approx 0$ (where the z axis is the threefold axis), which can be derived from the properties of the **G** vector.[8] This kind of interaction perturbs only the two lowest Kramers doublets of the $S_T = {}^1/_2$ system, and diagonalization yields the following energy levels:

$$E = \pm\frac{\left[\Delta E^2 + |M|^2 \pm 2\sqrt{\delta^2|M|^2 + |M\cdot G|^2}\right]^{1/2}}{2} \quad (5)$$

where $|M| = (g_{xy}{}^2\sin^2\theta + g_z{}^2\cos^2\theta)^{1/2}\beta H$ is the Zeeman term, $|G| = \sqrt{3}|G_z|$ (assuming that $|G_x| = |G_y| \approx 0$, which is valid for a weakly axial system with $J_{12} \approx J_{23}$), $|M\cdot G| = 4\sqrt{3}G_z g_z \beta H\cos\theta$, $\delta = |J_0 - J_1|$, and $\Delta E = (\delta^2 + |G|^2)^{1/2}$. It must be pointed out that the sign of **G** is also undefined under these conditions. It has been shown that the $S_T = {}^3/_2$ state is not perturbed by the antisymmetric exchange (**G**) term and does not affect the description of the $S_T = {}^1/_2$ states. Using the approach outlined in ref 3b, we were able to fit the low-temperature (1.8−8 K) data, and the fitting results are shown in Figure 4 as solid lines while the resulting fitting parameters are $g_{xy} = g_z = 2.1$ (fixed), $|G_z| = 20(1)$ cm^{-1}, $\delta = 40(2)$ cm^{-1}.

Magnetization data over the field range 0−6.5 T at 2 K are shown in Figure 5 along with the Brillouin function for an $S_T = {}^1/_2$ system with $g = 2.1$ (dotted line). The discrepancy between the Brillouin curve and the experiment

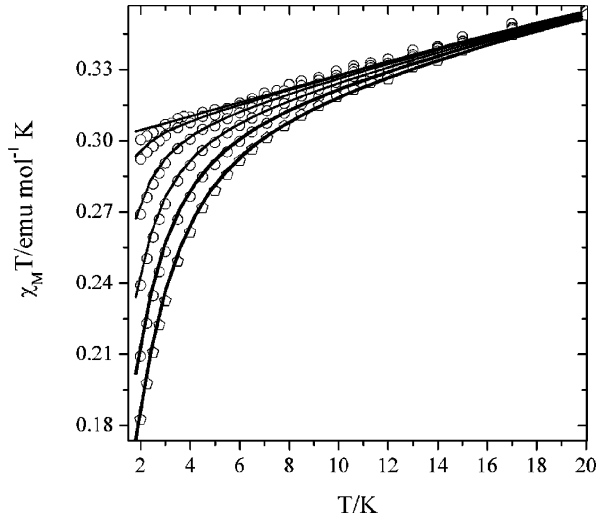

Figure 4. Low-temperature susceptibility data for **1** in the form of $\chi_M T$-versus-T plots corresponding from top to bottom to external fields ranging from 0 to 5 T. The solid lines represent the fitting results obtained using the Hamiltonian given in eq 4.

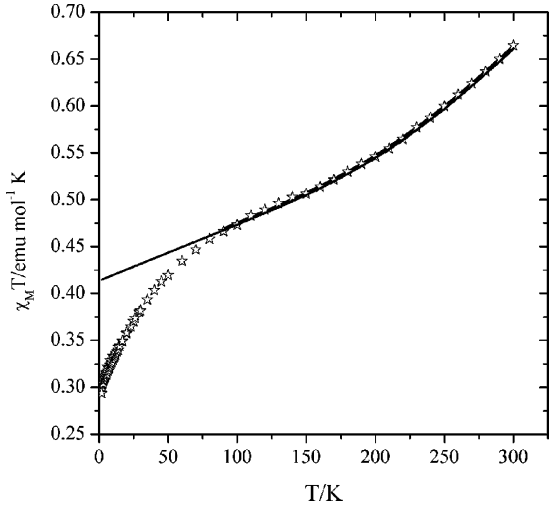

Figure 3. Temperature dependence of the magnetic susceptibility of **1**. The solid line shown with the experimental $\chi_M T$ data (☆) is the theoretical curve derived from the Hamiltonian given in eq 3.

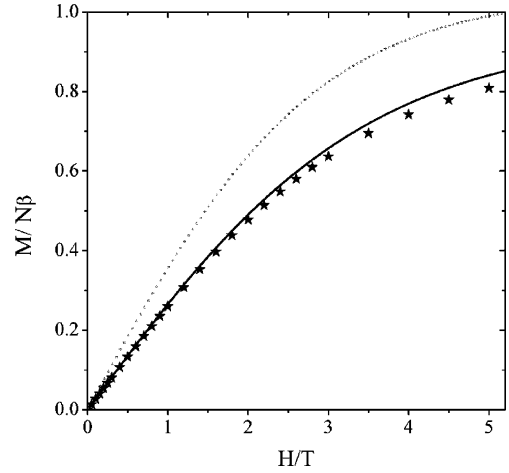

Figure 5. Magnetization data over the field range 0−6.5 T at 2 K for **1**. The dotted line is the Brillouin function for an $S = {}^1/_2$ system with $g = 2.1$, while the solid line was obtained from the magnetization formula modified with the addition of antisymmetric terms.

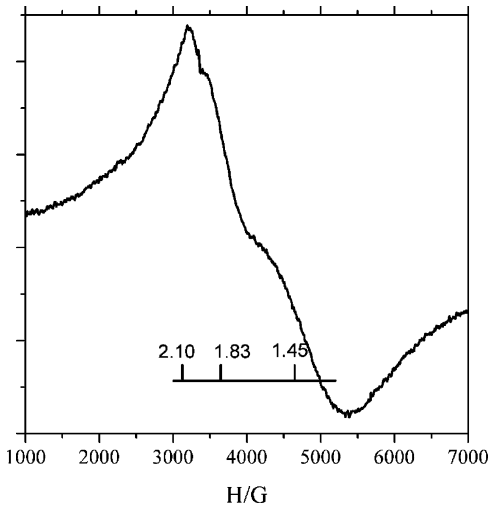

Figure 6. EPR spectrum of a polycrystalline sample of **1** recorded at 4 K. Other EPR conditions: modulation amplitude, $10G_{pp}$; microwave frequency, 9.48 GHz.

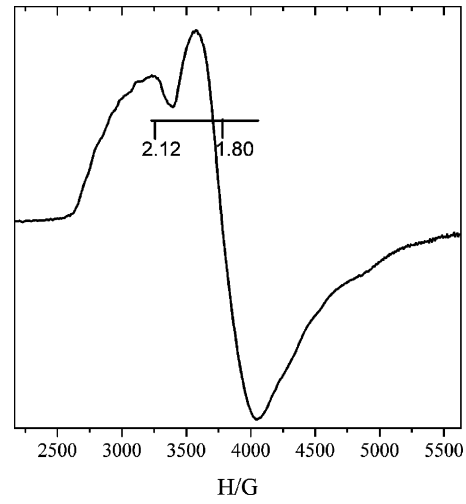

Figure 7. EPR spectrum of a sample of **1** in DMF solution, recorded at 4.2 K. Other EPR conditions: modulation amplitude, $10G_{pp}$; microwave frequency, 9.48 GHz.

provides clear evidence of the influence of the antisymmetric interaction. Introducing the antisymmetric terms derived from the fit of the susceptibility data into the magnetization formula caused the simulated curve to become nearly superimposable on the experimental one.

EPR Spectroscopy. The powder EPR spectrum of a polycrystalline sample of complex **1** at 4 K is shown in Figure 6. The powder spectrum reveals an absorption peak at $g = 2.10$ accompanied by a derivative feature at $g = 1.45$. A weaker feature (shoulder) also appears at $g_{eff} = 1.83$. This spectrum can be satisfactorily reproduced by assuming a distribution of axial species with $g_{||}$ fixed at 2.10 and $g_{\perp}$ varying from 2.10 to 1.40.[9]

The EPR spectrum of a polycrystalline sample of complex **1** in DMF solution at 4.2 K is shown in Figure 7; an absorption peak at $g_{eff} = 2.12$ accompanied by a broad transition centered at $g_{eff} = 1.80$ is observed. We attributed these signals to an $S = {}^1/_2$ state with axial **g**-tensor components $(g_{||}, g_{\perp}) = (2.12, 1.80)$. The solution spectrum is more axial than the powder one but still reveals an important **g** anisotropy and shows that the structure is retained. The large anisotropy in the **g** tensor with the rather small $g_{\perp}$ value for the $S = {}^1/_2$ ground state is usually attributed to the effect of an antisymmetric exchange interaction, according to eq 4.[8,10] The effect of this antisymmetric interaction is to induce an axial anisotropy in the **g** tensor.

More explicitly, the $g_{||}$ component is not affected, whereas a shift toward lower g values is observed for the $g_{\perp}$ component. The EPR findings show that the compound **1** has isosceles magnetic symmetry or lower ($\delta \neq 0$) and that antisymmetric exchange is important ($\mathbf{G} \neq 0$) and $\Delta E > h\nu$. The resulting relationship is:[3b,11]

$$g_{\perp} = g_0\left[\frac{\delta^2 - (h\nu)^2}{\Delta E^2 - (h\nu)^2}\right]^{1/2} \quad (6)$$

where $h\nu$ is the microwave energy ($\approx$0.31 cm^{-1}), g_0 is the true value of $g_{\perp}$ ($\sim$2.1 according to the susceptibility data), and, as before, $|G| = \sqrt{3}|G_z|$ and $\Delta E = (\delta^2 + |G|^2)^{1/2}$, with the δ and G_z factors calculated from the fit to the susceptibility data. According to these fitting results, $g_{\perp}/g_0 = 0.75$, which is close to the value obtained from the powder EPR spectrum (0.69).[12] This is clear evidence that the susceptibility results are in accordance with the EPR findings.

Magnetostructural Correlations. The magnetic exchange interaction in a triangular arrangement of three $S = {}^1/_2$ ions results in three electronic states, that is, a spin-frustrated state ($S = {}^1/_2$, doubly degenerate, ^{2}E) and a quartet state ($S = {}^3/_2$, $^4A_2$) corresponding to the antiferromagnetic and ferromagnetic complexes, respectively (Scheme 2).

In view of the fact that the three copper(II) atoms of the triangular Cu_3 cores in **1**, **2**, $[Cu_3(PhPyCNO)_3(OH)(CH_3OH)_2(ClO_4)_2]$ (**3**), and $[Cu_3(PhPyCNO)_3(\mu_3\text{-OMe})(Cl)(ClO_4)]$ (**4**) as well as in the model complexes $[Cu_3(\kappa^3N,N,O\text{-HNCHCHNO})_3(\mu_3\text{-O})(\mu_2\text{-HCOO})(HCOO)]$ (**5**), $[Cu_3(\kappa^3N,N,O\text{-HNCHCHNO})_3(\mu_2\text{-HCOO})(HCOO)]^+$ (**6**), $[Cu_3(\kappa^3N,N,O\text{-HNCHCHNO})_3(\mu_3\text{-O})]^+$ (**7**), and $[Cu_3(\kappa^3N,N,O\text{-HNCHCHNO})_3]^{3+}$ (**8**) are structurally almost equivalent (the distances between the magnetic ions in all of these complexes are similar), the three J_{ij} constants in the model of an isotropic exchange interaction for a quasi-equilateral triangle should be equal ($J_{12} = J_{13} = J_{23} = J$). For the symmetric trimers, the quartet ($^4A_2$) and doublet (^{2}E) states are separated by $3|J|$ in energy.[5p] We have also used the approximate generalized spin-projection method

(8) (a) Tsukerblat, B. S.; Belinskii, M. I.; Fainzil'berg, V. I. *Sov. Sci. Rev., Sect. B.* **1987**, *9*, 337–481. (b) Tsukerblat, B. S.; Kuyavskaya, B. Y.; Belinskii, A. V.; Novotortsev, V. M.; Kallinikov, V. T. *Theor. Chim. Acta* **1975**, *38*, 131–138.

(9) Vlachos, A.; Psycharis, V. C.; Raptopoulou, P.; Lalioti, N.; Sanakis, Y.; Diamantopoulos, G.; Fardis, M.; Karayanni, M.; Papavassiliou, G.; Terzis, A. *Inorg. Chim. Acta* **2004**, *357*, 3162–3172.

(10) Bencini, A.; Gatteschi, D. *EPR of Exchange Coupled Systems*; Springer-Verlag: Berlin, 1990.

(11) Rakitin, Y. V.; Yablokov, Y. V.; Zelentsov, V. V. *J. Magn. Reson.* **1981**, *43*, 288–301.

(12) The assumption that $g_{\perp} = g_{min} = 1.45$ was made.

Scheme 2. Energy Diagram for an Antiferromagnetically Coupled ($J < 0$) Cu(II) Trimer with Three Bridging Ligands

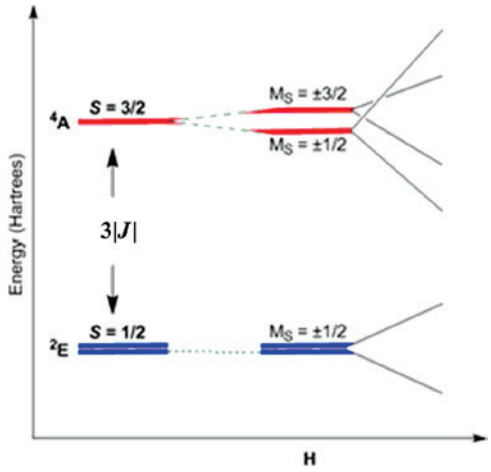

proposed by Yamaguchi et al.,[13] which is valid for two or three magnetic centers and relies upon the dependence of the exchange coupling parameter J on the spin contamination of the broken-symmetry (BS) solution:

$$J = -\frac{E_{HS} - E_{LS}}{\langle S^2\rangle_{HS} - \langle S^2\rangle_{LS}}$$

where E_{HS} and E_{LS} denote the total energies of the high-spin (HS) and low-spin (LS) states, respectively, while $\langle S^2\rangle_{HS}$ and $\langle S^2\rangle_{LS}$ denote the squares of the magnitudes of the total spins of the HS and LS states, respectively. At a practical level, calculations on the HS ($S = {}^3/_2$) and LS ($S = {}^1/_2$) states were performed using density functional theory (DFT) at the B3LYP level together with the basis set of triple-ζ quality proposed by Schaefer et al.[14] (TZP) for the copper atoms and a 6−31G(d) basis set for the remaining nonmetal atoms. We applied the aforementioned computational scheme on the basis of its excellent performance for the calculation of magnetic exchange coupling constants in polynuclear magnetic systems.[15] Theoretical calculations based on DFT were performed using the full crystal structures of **1**−**4**. We fully optimized the geometries of both the doublet and quartet states of the model compounds **5**, **6**, and **7** at the same level of theory, and vibrational analysis indicated that the resulting equilibrium geometries corresponded to minima on the potential energy surface. The equilibrium geometries of the model compounds **5**, **6**, and **7** in their doublet ground states along with selected structural parameters and the atom numbering scheme are shown in Figure 8. The calculations were performed using the Gaussian 03 code.[16]

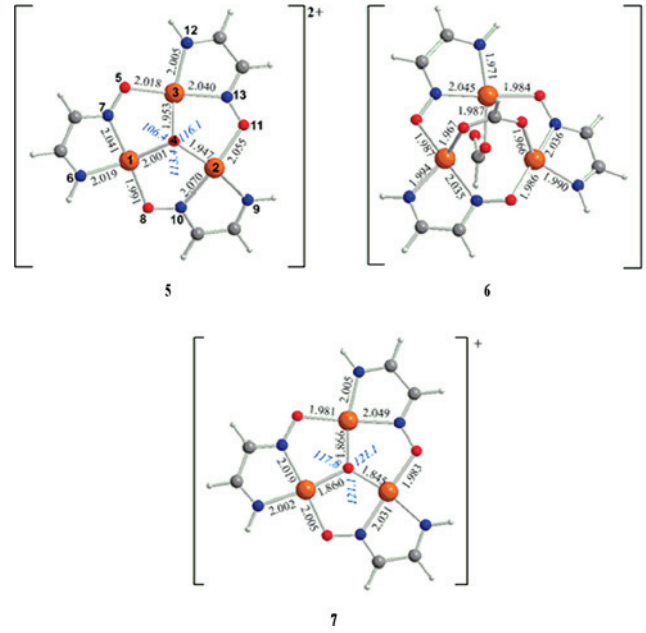

Figure 8. Equilibrium geometries of the model compounds **5**, **6**, and **7** along with selected bond lengths (Å) and bond angles (deg) and the atom numbering scheme. For the sake of clarity, the formate groups and the hydrogen atom of the hydroxide ligand have been omitted in **5**.

Removal of the triply bridging hydroxide ligand did not significantly alter the triangular Cu_3 structural core. The Cu(1)···Cu(2), Cu(1)···Cu(3), and Cu(2)···Cu(3) distances in **5** (**6**) are 3.311 (3.298), 3.160 (3.167), and 3.300 Å (3.309 Å), respectively. On the other hand, model **7** adopts a perfect planar configuration with the triply bridging oxo ligand at the centroid of the Cu_3 triangle.

The Cu(1)···Cu(2), Cu(1)···Cu(3), and Cu(2)···Cu(3) distances in **7**, which were found to be 3.227, 3.190, and 3.231 Å, respectively, indicate that the Cu_3 triangle could be considered as a nearly equilateral triangle, with the model complex **7** belonging to the C_{3h} point group.

Table 4 gives the total energies E_{HS} and E_{LS}, values of $\langle S^2\rangle_{HS}$ and $\langle S^2\rangle_{LS}$, distances of the μ_3-O atom from the centroid of the Cu_3 triangle (R), and corresponding isotropic exchange constant (J) values (estimated using both Yamaguchi's model and the formula $3|J| = E_{HS} - E_{LS}$) for compounds **1**−**8**.

It can be seen that the calculated J values, in particular those estimated using the formula $3|J| = E_{HS} - E_{LS}$, show good agreement with those obtained experimentally. Moreover, it is clear that using different carboxylate ligands does not appear to introduce significant changes in the exchange couplings. The magnetic exchange pathway is primarily mediated by the oximato (μ_2-NO) and the triply bridging oxo or hydroxide (μ_3-O or μ_3-OH) ligands, and both of these mediators support an antiferromagnetic interaction. However,

(13) (a) Shoji, M.; Koizumi, K.; Kitagawa, Y.; Kawakami, T.; Yamanaka, S.; Okumura, M.; Yamaguchi, K. *Chem. Phys. Lett.* **2006**, *432*, 343–347. (b) Soda, T.; Kitagawa, Y.; Onishi, T.; Takano, Y.; Shigeta, Y.; Nagao, H.; Yoshioka, Y.; Yamaguchi, K. *Chem. Phys. Lett.* **2000**, *319*, 223–230. (c) Yamaguchi, K.; Jensen, F.; Dorigo, A.; Houk, K. N. *Chem. Phys. Lett.* **1988**, *149*, 537–542.

(14) Schaefer, A.; Huber, C.; Ahlrichs, R. *J. Chem. Phys.* **1994**, *100*, 5829–5835.

(15) (a) Ruiz, E.; Alvarez, S.; Cano, J.; Polo, V. *J. Chem. Phys.* **2005**, *123*, 164110–164117. (b) Ruiz, E.; Alvarez, S.; Rodríguez-Fortea, A.; Alemany, P.; Pouillon, Y.; Massobrio, C. In *Magnetism: Molecules to Materials*; Miller, J. S., Drillon, M., Eds.; Wiley-VCH: Weinheim, Germany, 2001; Vol. *2*, p 227.

(16) Frisch, M. J.; et al. *Gaussian 03*, revision B.03; Gaussian, Inc.: Pittsburgh, PA, 2003. The full citation is given in the Supporting Information.

Table 4. Total Energies (E_{HS} and E_{LS}), $\langle S^2\rangle$ and $\langle S^2\rangle_{LS}$ Values, Distances of the μ_3-O Atom from the Centroid of the Cu_3 Triangle (R), and Corresponding Isotropic Exchange Constant (J) Values in **1**−**8**

property	**1**	**2**	**3**	**4**	**5**	**6**	**7**	**8**
E_{HS} (hartree)	−10765.49136	−7013.81522	−6938.68764	−7437.64464	−6164.01742	−6087.88856	−5784.86767	−5708.69712
E_{LS} (hartree)	−10765.49491	−7013.81872	−6938.69202	−7437.64806	−6164.02129	−6087.88971	−5784.88063	−5708.70810
$\langle S^2\rangle_{HS}$ (au)	3.75914	3.75966	3.76021	3.75975	3.75896	3.770597	3.760981	3.818913
$\langle S^2\rangle_{LS}$ (au)	1.67917	1.67353	1.65428	1.67858	1.66985	1.682877	1.504219	1.429488
R (Å)	0.66	0.68	0.59	0.893	0.574	–	0.000	–
J_{calc} (cm^{-1})[a]	−374.6 (−259.7)	−368.3 (−256.1)	−456.5 (−320.4)	−360.7 (−250.2)	−406.6 (−283.1)	−261.7 (−84.1)	−1260.9 (−948.1)	−1008.5 (−803.3)
J_{exp} (cm^{-1})	−220	–	–	−400	–	–	–	–

[a] Values in parentheses were estimated using the formula $|J| = (E_{HS} - E_{LS})/3$.

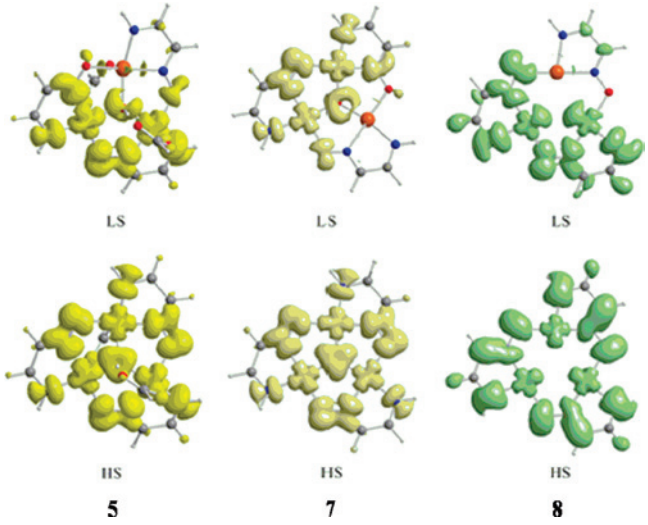

Figure 9. Representations of the spin density maps of the model complexes **5**, **7**, and **8** in their LS doublet and HS quartet states computed at the B3LYP/TZP(Cu)∪6−31G(d)(E) level of theory. The isodensity surfaces represented correspond to a value of 0.001 e/b^3.

the bridging carboxylato ligands could also participate in the exchange pathway, introducing (probably to a lesser extent) a countercomplementarity effect.[17]

To understand the unexpectedly large antiferromagnetic interaction in this family of compounds, we analyzed the distributions of the spin densities in the LS doublet ground and HS quartet excited states. The atomic spin densities of these two states in the trinuclear Cu(II) complexes are compiled in Table S1 in the Supporting Information, while the spin density distributions of the representative model complexes **5**, **7**, and **8** are depicted in Figure 9. It can be seen that for the most part, the spin density is localized almost equally on the three copper(II) cations, which could be considered as equivalent magnetic centers in an equilateral triangular environment.

Significant spin delocalization toward the bridging nitrogen and oxygen donor atoms is associated with the bonding and antibonding combinations of the $3d_{x^2-y^2}$ orbitals bearing the unpaired electrons (Scheme 3). These singly occupied molecular orbitals (SOMOs) favor the coupling of the unpaired electrons, and consequently, the doublet state is stabilized. In each Cu(II) magnetic center having C_{4v} symmetry, all of the magnetic orbitals of a_1 ($3d_{z^2}$), b_1 ($3d_{x^2-y^2}$), b_2 ($3d_{xy}$) and e ($3d_{xz}$, $3d_{yz}$) symmetry seem to contribute to the magnetic exchange coupling. The a_1 and e magnetic orbitals, although less important,

(17) (a) Kahn, O. *Molecular Magnetism*; VCH Publishers, Inc.: New York, 1993. (b) Gutierrez, L.; Alzuet, G.; Real, J. A.; Cano, J.; Borras, J.; Castineiras, A. *Inorg. Chem.* **2000**, *39*, 3608–3614.

Scheme 3. Bonding and Antibonding Combinations of the $3d_{x^2-y^2}$ Singly Occupied Molecular Orbitals (SOMOs) of the Model Trinuclear Cu(II) complexes **4**, **5**, **7**, and **8**

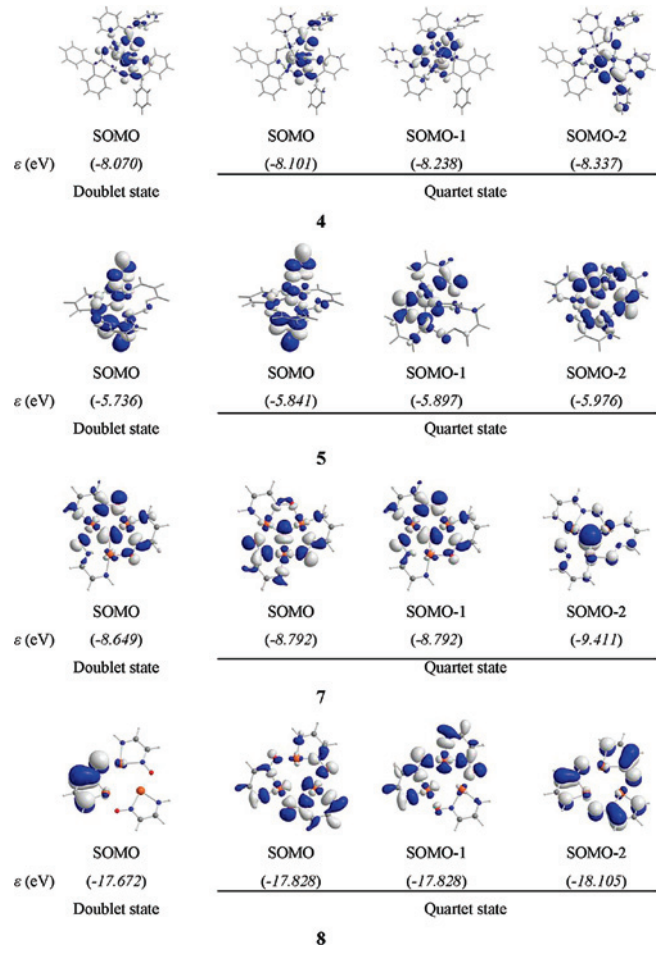

might overlap with the p-type orbitals of the central triply bridging oxide ligand, thereby affecting its displacement from the Cu_3 plane and contributing to the antiferromagnetic coupling.

The plots of the SOMOs clearly reflect the main role of the oximato −N−O− bridges in the unexpectedly large antiferromagnetic exchange interaction, because a large spin density at the bridging ligand in turn favors strong antiferromagnetic coupling. The O and N donor atoms of the −N−O− bridges acquire spin density distributions of 0.096−0.137 and 0.056−0.118 e/b^3, respectively (Table 4). The magnetic orbitals supporting the antiferromagnetic coupling correspond to the SOMO and SOMO-1 that result from out-of-phase interactions of π^*-type MOs localized on the −N−O− bridges with the appropriate symmetry-adapted combinations of the $3d_{x^2-y^2}$ or $3d_{z^2}$ orbitals of the three Cu(II) magnetic centers. These magnetic orbitals, which mediate

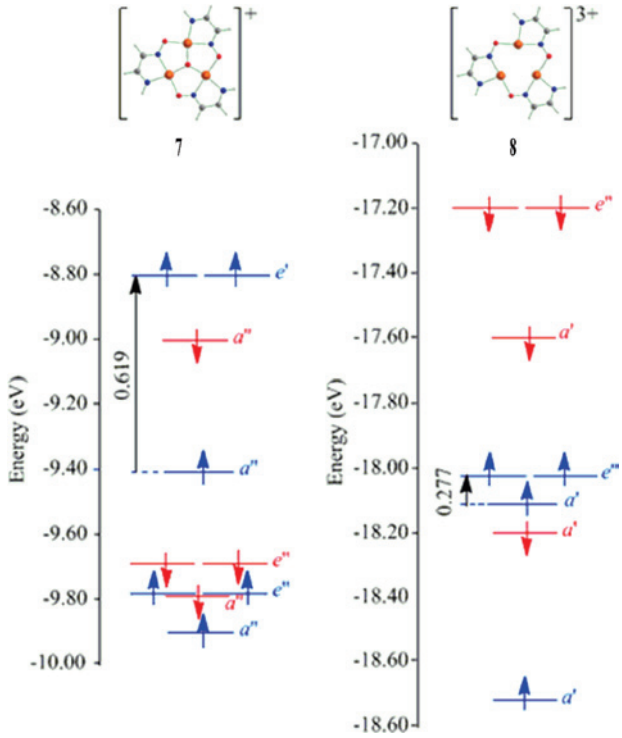

Figure 10. Energy-level diagrams for the FMOs obtained from DFT calculations on the C_{3h} model complexes **7** (containing a μ_3-O ligand) and **8** (without a μ_3-O ligand).

the antiferromagnetic exchange coupling exclusively via the oximato −N−O− bridges, are clearly shown in Scheme 3 for the model complex **8**. The SOMO and SOMO-1 magnetic orbitals also involve antibonding interactions between the in-plane p_x and p_y orbitals of the μ_3-O ligand and the appropriate symmetry-adapted combinations of the $3d_{x^2-y^2}$ or $3d_{xy}$ orbitals of the three Cu(II) magnetic centers. These magnetic orbitals are clearly shown in the contour plots of the e″ SOMO and SOMO-1 of model complex **7**, in which the μ_3-O ligand lies in the Cu_3 plane (Scheme 3).

The μ_3-O ligands contribute significantly to the large antiferromagnetic exchange interaction, as evidenced by their significant spin densities of 0.198−0.403 e/b^3. The features of the frontier molecular orbital (FMO) energy-level diagrams for model complexes **7** and **8** are presented in Figure 10. In complex **7**, in which the μ_3-O ligand lies in the Cu_3 plane, the bonding σ(Cu−O) interactions are lost and the SOMO-2 energy is stabilized, thus increasing the SOMO/SOMO-2 energy gap (as shown by a comparison of the SOMO/SOMO-2 energy gaps in the FMO energy-level diagrams for complexes **7** and **8** in Figure 10). In effect, the antiferromagnetic contribution, which is proportional to the square of the SOMO/SOMO-2 energy gap,[18] dominates the ferromagnetic contribution, stabilizing the ^{2}E ground state. It is interesting to note that the contribution of the in-plane μ_3-O ligand to the antiferromagnetic exchange coupling in model complex **7** amounts to 20%.

A magnetic orbital that further supports the antiferromagnetic coupling is SOMO-2 in complexes **4** and **7** (Scheme 3). This magnetic orbital in the planar model complex **7** is an a″ π*-type MO resulting from the out-of-phase interaction of the oxygen p_z AO with the a″ combination of the three $3d_{xz}$ or $3d_{yz}$ orbitals of the Cu(II) magnetic centers. The weaker antiferromagnetic coupling in **4**, which also involves a triply bridging chloride (μ_3-Cl) ligand, is noteworthy as well. This could be due to a countercomplementarity effect, since the SOMOs of the doublet ground and quartet excited states correspond to antibonding molecular orbitals localized primarily on the chloride ligand, and/or to structural changes introduced by the μ_3-Cl ligand, which pushes the μ_3-OMe ligand further away from the centroid of the triangular Cu_3 ring. It should be noted that the μ_3-Cl ligand acquires spin densities of 0.021 and 0.031 e/b^3 in the doublet and quartet states, respectively. Moreover, the geometry of the trigonal bipyramidal $Cu_3(\mu_3\text{-OMe})(\mu_3\text{-Cl})$ core of **4** allows only the overlap of the Cu(II) 3d and μ_3-Cl p_x and p_y AOs, which is consistent with ferromagnetic exchange coupling among the three Cu-centers that might be responsible for the decrease in the antiferromagnetic coupling constant J in **4**. Finally, the oxygen donor atoms of the carboxylate ligands have no electron spin density at all (their electron spin densities range from −0.0003 to 0.007 e/b^3), and therefore, their contribution to the antiferomagnetic coupling is actually negligible. However, weak antibonding interactions still exist between the p_x and p_y orbitals localized on the oxygen donor atoms of the carboxylate ligands and the appropriate symmetry-adapted combinations of the 3d orbitals of the three Cu(II) magnetic centers. The countercomplementarity effect of the bridging formato ligands in model complex **6**, which accounts for the weaker estimated antiferromagnetic coupling in **6** than in **8**, is also noteworthy.

The crucial role of the μ_3-O ligand on the antiferromagnetic exchange coupling between the three Cu(II) magnetic centers is further evidenced by the excellent linear correlation of the coupling constant J with the distance of the μ_3-O from the centroid of the Cu_3 triangle, as shown in Figure 11. The linear relationships in panels a and b of Figure 11 predict that at $R = 0$, the J value would be −1260.7 or −937.4 cm^{-1}, respectively, and that J would become zero at R = 0.852 or 0.879 Å, respectively. It is evident that the small structural distortions related to the structural parameter R in conjunction with the nature of the bridging ligands play a significant role in the switch from antiferromagnetic to ferromagnetic exchange in the family of the oximato-based $[Cu_3(\mu_2\text{-N=O})(\mu_3\text{-O})]$ triangular complexes. On the basis of the linear relationships in Figure 11, using the measured value of 0.352 Å for R, we predict a J value of −740.1 or −562 cm^{-1}, respectively, for the analogous complex $[\{Cu_3(O)L_3(ClO_4)\}_2]$ [L = 1,2-diphenyl-2-(methylimino)ethanone-1-oxime], which exhibits the greatest antiferromagnetic J value (∼1000 cm^{-1}) reported to date.[19]

Conclusions

We have demonstrated in this work that phenyl 2-pyridyl ketoxime (PhPyCNOH) can serve as a scaffold for the

(18) Hay, P. J.; Thibeault, J. C.; Hoffmann, R. *J. Am. Chem. Soc.* **1975**, *97*, 4884–4899.

(19) Butcher, R. J.; O'Connor, C. J.; Sinn, E. *Inorg. Chem.* **1981**, *20*, 537.

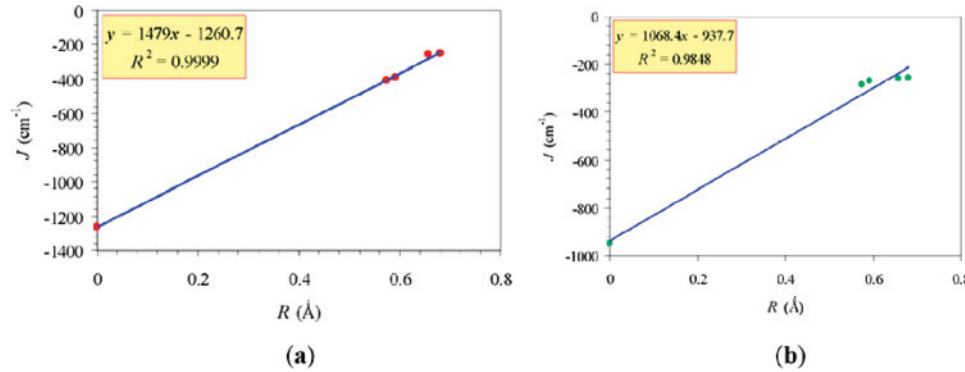

Figure 11. Linear correlation of the coupling constant J, estimated using (a) Yamaguchi's model and (b) the formula $3|J| = E_{HS} - E_{LS}$, with R, the distance of the μ_3-O ligand from the centroid of the Cu_3 triangle.

formation of inverse-9-metallacrown-3 complexes accommodating one or two anions. The magnetic behavior showed a large antiferromagnetic interaction. In view of the fact that the distances between the magnetic ions in complex **1** are almost the same, implying that the three J_{ij} constants should be equal, it was difficult to resolve the exact value of this large antiferromagnetic interaction. In order to clarify the low-temperature behavior, systematic measurements of the susceptibility were carried out at different magnetic fields; the results showed that the $S_T = {}^3/_2$ state is not perturbed by the antisymmetric exchange (**G**) term and does not affect the description of the $S_T = {}^1/_2$ states. The discrepancy between the Brillouin curve and the experimental results provided clear evidence of the influence of the antisymmetric interaction. Introducing the antisymmetric terms derived from the fit of the susceptibility data into the magnetization formula caused the simulated curve to become nearly superimposable on the experimental one. The EPR findings showed that compound **1** has isosceles or lower magnetic symmetry ($\delta \neq 0$) and that antisymmetric exchange is important ($\mathbf{G} \neq 0$) and $\Delta E > h\nu$. Theoretical calculations based on DFT were performed using crystal structures and model compounds; the structures of both the doublet and quartet states were optimized at the same level of theory, and vibrational analysis indicated that the resulting equilibrium geometries corresponded to minima on the potential energy surface. Both e_g and t_{2g} magnetic orbitals seem to contribute to the magnetic exchange coupling. The latter contribution, although less important, might be due to overlap of the t_{2g} orbitals with the p-type orbitals of the central triply bridging oxide ligand, thereby affecting its displacement from the Cu_3 plane and contributing to the antiferromagnetic coupling. The crucial role of the μ_3-O ligand on the antiferromagnetic exchange coupling between the three Cu(II) magnetic centers was further evidenced by the excellent linear correlation of the coupling constant J with the distance of the μ_3-O ligand from the centroid of the Cu_3 triangle.

Acknowledgment. This project was cofunded by the European Social Fund of the European Union "Pythagoras II".

Supporting Information Available: CIF files for **1** and **2**, complete citation for ref 16, and atomic spin densities (Table S1) and Cartesian coordinates and energy data (Table S2) for the trinuclear Cu(II) complexes. This material is available free of charge via the Internet at http://pubs.acs.org.

IC8003257